

Ehrlich-Schwöbel effect on the growth dynamics of GaAs(111)A surfaces

Luca Esposito,¹ Sergio Bietti,¹ Alexey Fedorov,² Richard Nötzel,^{3,1} and Stefano Sanguinetti^{1,2,*}

¹*L-NESS and Department of Materials Science, University of Milano-Bicocca, 20125 Milano, Italy*

²*L-NESS and CNR-IFN Institute, 22100 Como, Italy*

³*South China University of Technology, 510630 Guangzhou, China*

(Received 31 August 2016; published 5 July 2017)

We present a detailed characterization of the growth dynamics of Ga(Al)As(111)A surfaces. We develop a theoretical growth model that well describes the observed behavior on the growth parameters and underlines the Ehrlich-Schwöbel barrier as a leading factor that determines the growth dynamics. On such basis we analyze the factors that lead to the huge observed roughness on such surface orientations and we identify the growth conditions that drive the typical three-dimensional growth of Ga(Al)As(111)A towards an atomically flat surface. GaAs/Al_{0.30}Ga_{0.70}As quantum wells realized on an optimized surface (<0.2 nm roughness) show a record low emission linewidth of 4.5 meV.

DOI: [10.1103/PhysRevMaterials.1.024602](https://doi.org/10.1103/PhysRevMaterials.1.024602)

I. INTRODUCTION

In the field of semiconductor nanotechnology for transport and optoelectronic applications there are cases where the employment of non-(100) surfaces improves the characteristics of the device or can even be a necessary condition for its functioning. Among crystalline surfaces the (111) is the one that has gathered more attention in the last years, especially for what concerned the optoelectronic applications of III-V semiconductors. Its physical and geometrical characteristics, in fact, are particularly suitable for devices such as high-mobility transistors (HMTs) [1–3] and quantum well (QW) intersubband photodetectors [4], but also for the feasible implementation of a new generation of devices like the ones based on topological insulators [5], spintronics [6–10], and entangled photons [11–17].

However, although high control on surface growth phenomena is a fundamental factor to avoid spurious and detrimental effects, such as fine-structure splitting for entangled-photon generation or carrier-mobility reduction for HMTs, studies regarding the growth of this surface are few, lacking an in depth description of growth mechanisms.

The (111) surface morphology, in most of the cases, is still affected by a large surface roughness. In particular, the growth of highly flat GaAs and AlGaAs (111)A surfaces, and consequently of high-quality nanostructures grown on this substrate, is strongly subordinated to the possibility of inhibiting the formation of large (with μm lateral dimensions) pyramidal hillocks with threefold symmetry, nucleated by stacking faults [18,19].

As a matter of fact, the growth, via molecular beam epitaxy (MBE), of Al_xGa_{1-x}As (111)A surfaces, with $0 \leq x \leq 0.3$, shows a complex behavior. A full explanation of the phenomenology cannot be given without a careful study of island growth dynamics. Here present a systematic study of the growth of Ga(Al)As(111)A to identify prominent adatom incorporation mechanisms, the model we built to understand and control the growth along this crystallographic direction, and the growth procedure we used to obtain atomically

flat (<0.2 nm rms) Al_{0.30}Ga_{0.70}As and GaAs (111)A surfaces. A fundamental role in determining the morphology of GaAs(111)A surfaces is played by the presence of a sizable Ehrlich-Schwöbel barrier [20,21] which promotes three-dimensional growth. The understanding of the growth dynamics on Ga(Al)As (111)A surfaces allowed us to obtain a quantum well with an extremely narrow emission linewidth on substrates with the [111] orientation.

II. METHODS

We fabricated and morphologically characterized twelve samples divided into three series, one for each of the free growth parameters we explored: (i) substrate temperature (T), (ii) group-III flux (F), and (iii) V/III beam-equivalent-pressure (BEP) ratio (Φ/F). See Table I for a summary of the sample growth conditions. All samples were grown with an MBE system on a (111)A semi-insulating GaAs substrate, with a nominal structure composed by a 10 nm GaAs buffer layer and a 100 nm Al_{0.30}Ga_{0.70}As epilayer. Both the buffer and the Al_{0.30}Ga_{0.70}As epilayer were grown at the same temperature.

After the growth, each sample was analyzed by an atomic force microscope (AFM) working in tapping mode, using tips with radius of curvature of 2 nm for the morphological characterization. The photoluminescence measurements of the fabricated QW were conducted at a temperature of 15 K and excited by a Nd:YAG laser, doubled in frequency, at 532 nm with a spot diameter of $\sim 300 \mu\text{m}$.

III. RESULTS

A typical AFM topographical image is presented in Fig. 1. We can clearly identify two families of pyramidal-shaped structures with different size and aspect ratios (the ratio between vertical over lateral dimensions), which are present in all the grown samples.

We will refer to the smaller structures as “islands” and to the big ones as “hillocks.” The roughness (in terms of rms) due to islands is quite small (~ 0.2 nm on an $8 \times 8 \mu\text{m}^2$ area) while the contribution given by hillocks can be huge (~ 2 nm) and their minimization is one of the points on which our study is focused.

*stefano.sanguinetti@unimib.it

TABLE I. Conditions used for the growth of the samples used in this work. Temperature, growth gate, and V/III BEP ratio series are indicated.

	Sample	T ($^{\circ}\text{C}$)	Group-III flux ($\text{s}^{-1}\text{cm}^{-2}$)	V/III ratio
Temperature	T1	460	6×10^{14}	75
	T2	490	6×10^{14}	75
	T3	520	6×10^{14}	75
	T4	550	6×10^{14}	75
Growth rate	G1	520	0.5×10^{14}	75
	G2	520	1.5×10^{14}	75
	G3	520	3×10^{14}	75
	G4	520	6×10^{14}	75
V/III ratio	R1	520	6×10^{14}	75
	R2	520	3×10^{14}	150
	R3	520	1.5×10^{14}	300
	R4	520	0.5×10^{14}	900

It is worth noting that all the results we obtained with the $\text{Al}_{0.30}\text{Ga}_{0.70}\text{As}$ epilayer are also valid for Al content lower than the 30%.

A. Temperature series

We explored the 460–550 $^{\circ}\text{C}$ temperature range (see Table I). At 460 $^{\circ}\text{C}$, as reported in Fig. 2(a), the growth of the $\text{Al}_{0.30}\text{Ga}_{0.70}\text{As}$ epilayer is 3D-like and the nucleated islands have the shape of rounded pyramids. Their average height is 2.5 nm with a base of 230 nm, and density of $1.8 \times 10^9\text{cm}^{-2}$. The hillocks, instead, have a shape that resembles an irregular shamrock, which is a typical symptom of dendritic growth on surfaces with C_3 symmetry [22]. The hillocks’ average height is 10 nm with a base of 130 nm and the density is $1.3 \times 10^8\text{cm}^{-2}$. The overall roughness (rms) on an $8 \times 8\ \mu\text{m}^2$ area is around 1.17 nm, while the “background rms” due to the islands’ corrugation is around 1 nm.

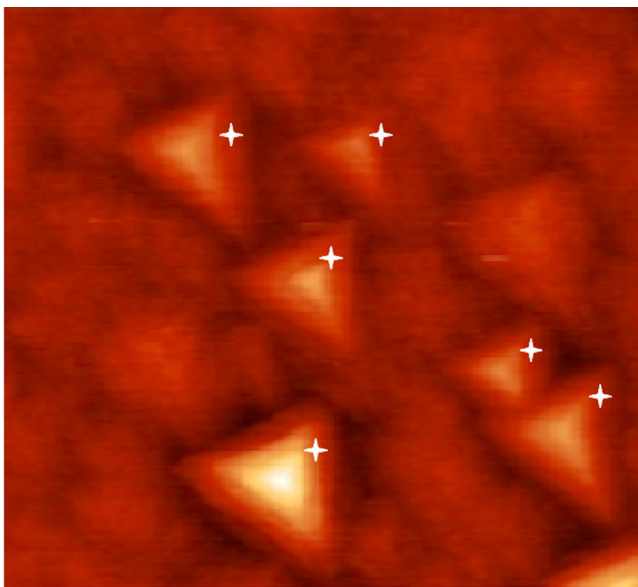


FIG. 1. AFM topographical image ($3 \times 3\ \mu\text{m}^2$) of sample G2. Hillocks are indicated by white stars.

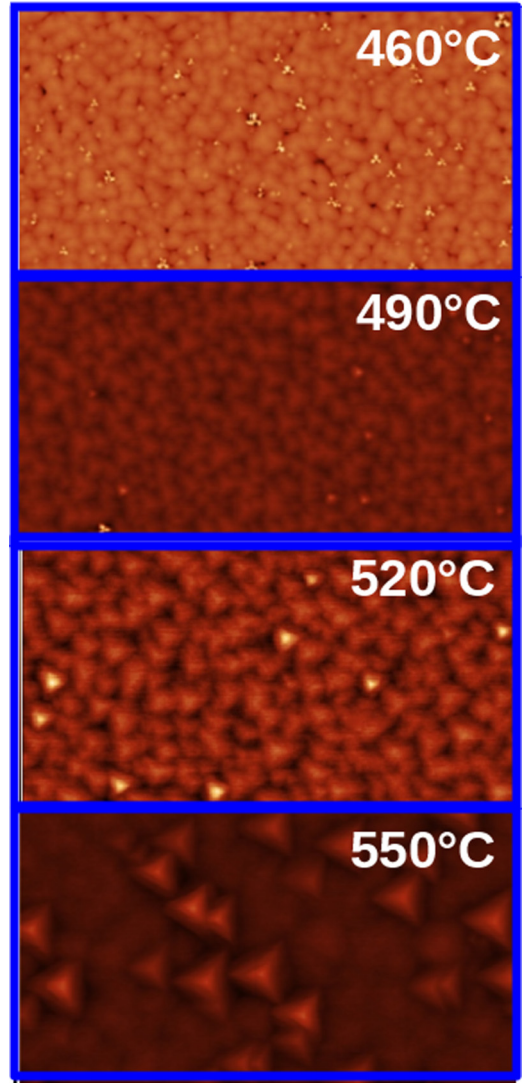


FIG. 2. AFM scans ($4 \times 8\ \mu\text{m}^2$) of the samples belonging to the temperature series: T1 (a), T2 (b), T3 (c), and T4 (d). The height scale in the images is from dark to bright with a maximum value of 30 nm (a), 21 nm (b), 7 nm (c), and 10 nm (d). Growth parameters are reported in Table I. The temperature ($^{\circ}\text{C}$) used in the growth is indicated in the panel.

Raising the temperature up to 490 $^{\circ}\text{C}$ [Fig. 2(b)], the sample growth enters a different regime. The islands and hillocks are regular triangular pyramids with net and definite sides. The average height, base, and density of the island are 1.2 nm, 304 nm, and $7.8 \times 10^8\text{cm}^{-2}$, respectively; for hillocks we measured 4.4 nm, 225 nm, and $4.5 \times 10^7\text{cm}^{-2}$, respectively. The overall rms on an $8 \times 8\ \mu\text{m}^2$ area is decreased to 0.6 nm while the background rms is 0.55 nm.

Increasing further the temperature [see Figs. 2(c) and 2(d)] the height and density of the islands are reduced but their base increases. A different behavior can be seen for hillocks, for which height increases as well as the base (although the aspect ratio still shows a reduction). Hillock density does not change significantly within the temperature series. The overall rms increases with the temperature due to the larger contribution from the hillocks to the value of 1.18 nm at 550 $^{\circ}\text{C}$. The background rms due to islands decreases to 0.4 nm.

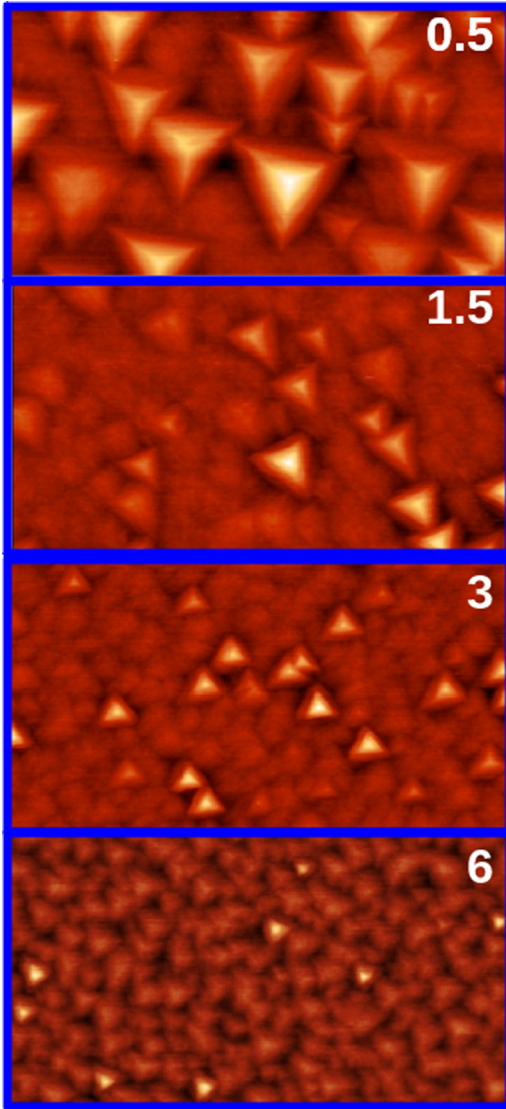


FIG. 3. AFM scans ($4 \times 8 \mu\text{m}^2$) of the samples belonging to the flux series: G1 (a), G2 (b), G3 (c), and G4 (d). The height scale in the images is from dark to bright with a maximum value of 16 nm (a), 12 nm (b), 11 nm (c), and 7 nm (d). Growth parameters are reported in Table I. The group-III flux ($\times 10^{14} \text{ cm}^{-2} \text{ s}^{-1}$) used in the growth is indicated in the panel.

B. Growth rate series

We explored the $0.5\text{--}6 \times 10^{14} \text{ atoms cm}^{-2}\text{s}^{-1}$ growth rate range (referred to as group-III adatoms) by changing simultaneously group-III and group-V flux but maintaining a constant V/III ratio (see Table I). At a rate of $0.5 \times 10^{14} \text{ atoms cm}^{-2} \text{ s}^{-1}$ big hillocks are observable with heights of more than 11 nm and a base of $1.5 \mu\text{m}$ [Fig. 3(a)]. The areas free from hillocks are quite small (less than $2 \mu\text{m}^2$) and on the latter the islands are almost completely merged. Because of that, no reliable statistics on islands can be made, although a low background roughness can be inferred from the 0.38 nm background rms (obtained excluding hillocks).

Increasing the growth rate [Figs. 3(b)–3(d)], hillocks become smaller, keeping their density basically constant. Accordingly, the overall rms decreases till the value of 0.57 nm

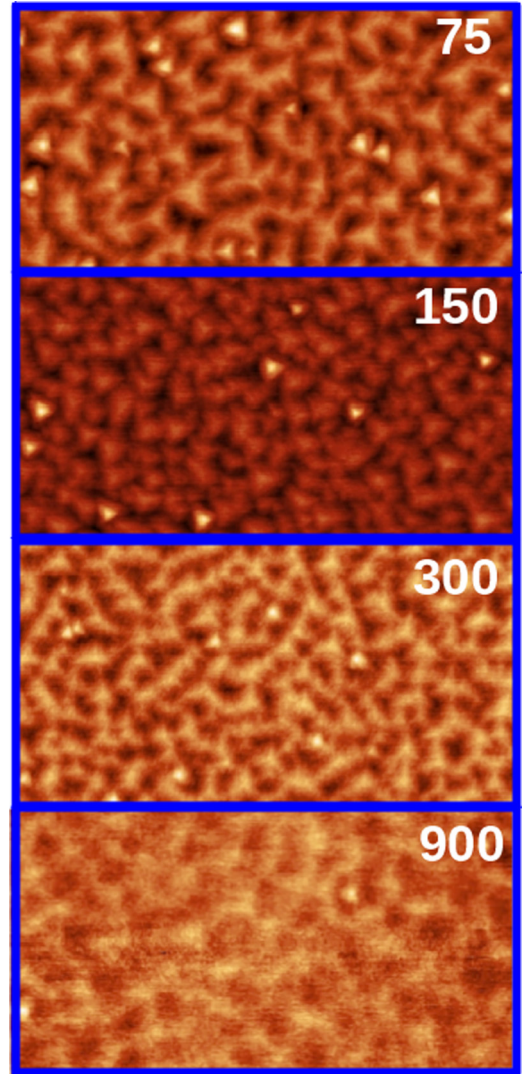


FIG. 4. AFM scans ($4 \times 8 \mu\text{m}^2$) of the samples belonging to the flux series R1 (a), R2 (b), R3 (c), and R4 (d). The height scale in the images is from dark to bright with a maximum value of 3 nm (a), 7 nm (b), 5 nm (c), and 2.5 nm (d). Growth parameters are reported in Table I. Φ/F , measured as As to Ga BEP ratio, used in the growth is indicated in the panel.

at $6 \times 10^{14} \text{ atoms cm}^{-2}\text{s}^{-1}$. For what concerns islands, the increase of the growth rate results in larger density and aspect ratio. This leads to a rise of the background rms.

C. V/III ratio series

The series spans the 75–900 BEP V/III ratio range. At a ratio of 75, which is the one used to realize the temperature and growth rate series, the growth is 3D-like with clearly distinguishable pyramidal hillocks. The overall rms is around 0.57 nm and the background one is around 0.47 nm [Fig. 4(a)].

Decreasing the group-III flux, in order to increase the V/III ratio till 300 [Fig. 4(c)], only a small change is observed in island density, which only reduces by a factor two, from 6 to $3.6 \times 10^8 \text{ cm}^{-2}$, when the V/III ratio increases from 75 to 300. The hillocks' density is around $3 \times 10^7 \text{ cm}^{-2}$ in the

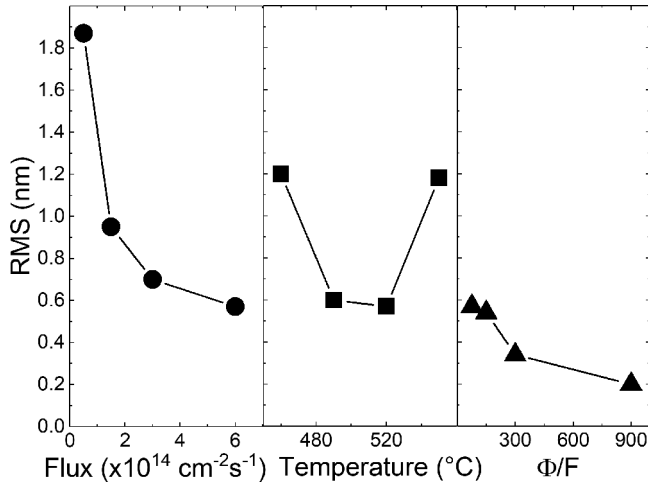


FIG. 5. Dependence of overall rms on the relevant growth parameters in growth rate (left panel), temperature (center panel), and V/III ratio (right panel) series.

whole range. However, the height of the two pyramid families decrease proportionally to V/III passing from an average value of 1.4 nm to 0.7 nm for islands, and from a value of 4.5 nm to 2.26 nm for hillocks.

Going further, to a V/III ratio of 900 [Fig. 4(d)] the regime of growth passes from 3D-like to 2D-like. The islands are practically one monolayer high and the hillocks, if present, are completely indistinguishable from islands. The overall rms (and obviously the background rms) drops to a value of 0.2 nm. The dependence of the rms on the relevant growth parameters in the three series is reported in Fig. 5.

IV. DISCUSSION

The description of the observed behavior of surface morphology, in terms of island rms, density (ρ), height, and aspect ratio (height over base ratio), is reported in Fig. 6. Some general trends can be identified. All the island relevant parameters tend to decrease with increasing temperature and group-V (Φ) over group-III (F) ratio, while the trend is reversed in the case of F dependence.

As a matter of fact, the variety of morphological observations in the three series resembles quite well what has been already reported in the literature on the homoepitaxial growth on (111)-oriented metals (Pt, Cu, Ag) [23] with an fcc lattice. In these materials the growth dynamics is quite well understood and extensive models based on a kinetic growth framework have been developed [21]. Within this scenario, it is natural to use the same basic concepts borrowed from the homoepitaxial growth of metals in the attempt of building an extended model for binary-alloy, such as III-As, materials, that could keep the same “predictive power” of the one made for metals.

The fundamental ingredient of (111) metal homoepitaxial models is the presence of a strong effective Ehrlich-Schwöbel (ES) barrier that, frustrating the escape of deposited adatoms from the top of a 2D nucleated island, drives the growth towards 3D. We suppose that the same phenomenon is playing a role in the observed behavior on GaAs. An estimation of the ES barrier on Ga(Al)As (111)A is not available in the literature.

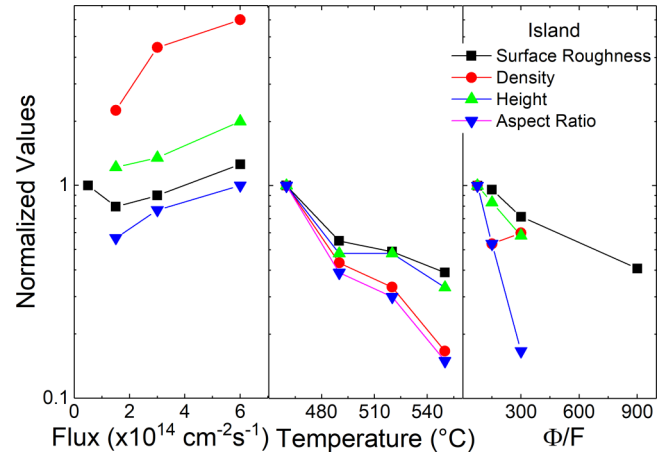


FIG. 6. Normalized dependence on the relevant growth parameter of island rms (black squares), density (ρ , red circles), height (green up-triangles), and aspect ratio (blue down-triangles) of the series and F (left panel), T (center panel), and Φ/F (right panel). The data are normalized to the one assumed at lowest value of the relevant growth parameter in the series.

However, a lower bound for the ES barrier will follow directly from *a posteriori* considerations after the construction of the model.

Before entering into the construction of the model it is worthwhile to give a qualitative picture of what happens during the epitaxial growth, in order to fix some fundamental ideas and define the needed parameters.

In a layer-by-layer regime, after an “initial delay time,” the adatoms impinging on the substrate surface start to aggregate and to form small 2D islands. After the nucleation of 2D islands, depending on the surface coverage and on single island size, the atoms coming from the cells have a certain probability of direct impingement onto the top of the freshly formed 2D islands.

In this case, after a time τ called the *residence time*, on which the adatom explores the island surface, three events can occur: (1) the adatom re-evaporates; (2) the adatom descends from the island top and eventually sticks on the step edge or starts the nucleation of a new island; (3) the adatom meets other adatoms and starts to nucleate a new island on the top of the previous one. Being in a complete condensation regime we will completely discard the re-evaporation processes. Depending on which of the two remaining events dominates, the growth will proceed 2D-like or 3D-like.

Assuming the case where the adatom diffusion is quite efficient and therefore the diffusion length l_D is larger than the average equivalent radius R of the 2D islands ($l_D \gg R$), the factor that can lead to multilayer nucleation is the ES barrier. A large value of the ES barrier, in fact, induces an increase of the residence time τ and an increase of the probability of adatoms encountering on the top of the island.

Within this kinetic framework three classes of parameters are important for the determination of the growth dynamics (see [21]):

- (1) the ones related to intralayer diffusion;
- (2) the ones related to the ES barrier;
- (3) the ones related to the growth parameters.

In the first class we find the diffusion length l_D , the diffusion time τ_D , and the diffusivity D . These parameters are related one to each other by the formula $l_D = \sqrt{4D\tau_D}$, where the rate for a diffusion process, depending on the temperature T and on the diffusion barrier E_D , is given by the law $\nu = \nu_0 e^{-\frac{E_D}{kT}}$, with ν_0 the attempt frequency.

In the second class we find the ES length $l_{ES} = (\frac{\nu}{\nu'} - 1)a$ and the ES time $\tau_{ES} = \frac{R}{2a\nu'}$, where a is the lattice parameter and, similarly to what is seen for the diffusion process, ν' is the rate of descending from the step edge regulated by the law $\nu' = \nu'_0 e^{-\frac{E_S}{kT}}$, where E_S is the sum of the E_D and of the ES barrier ΔE_S .

In the growth parameters class we have the temperature T , the flux of Ga F , and the flux of As Φ .

A. Description of the model

It is worth noting that all the growths were conducted in group-III limited conditions (As overpressure). In these conditions, once the As pressure is effectively taken into account in the value of diffusivity, the growth rate is completely determined by the group-III (Ga and/or Al) flux F only. For these reasons, using the term ‘‘adatom’’ we will refer to group-III adatoms only.

Moreover, similarly to what has been done for metals [21], we will assume that in our growth conditions the growth dynamics is not dominated by intrinsic (extremely low diffusivity) or extrinsic (high growth rate) limitation in the adatom’s diffusion path. These assumptions are not free from consequences and impose important bounds between the relevant time scales of our model.

In order to discard a diffusivity-limited dynamics, we should impose that the time elapsed by the adatom on the island edge trying to overcome the ES barrier and be incorporated in the island edge τ_{ES} is larger than the time needed to explore the island top surface τ_D : $\tau_{ES} \gg \tau_D$. This way the residence time τ , which is roughly the sum of the two contributions (τ_D^i and τ_{ES}), satisfies the condition $\tau \simeq \tau_{ES}$; that is, diffusivity dynamics plays only a minor role in determining the residence time. This condition remains true till the multilayer nucleation takes place on the top of a layer (for the second layer this is the base of the island, for the third this is the second layer, and so on) with radius $R \ll R_{cD}$, where R_{cD} is the critical radius for which $\tau_{ES} = \tau_D$:

$$\frac{R_{cD}^2}{4D} = \frac{R_{cD}}{2a\nu'} \mapsto R_{cD} = \frac{2D}{a\nu'}. \quad (1)$$

To discard dynamics limited by high growth rates, we should impose that the average delay time $\Delta t = \frac{1}{F\pi R^2}$ between the arrival of two adatoms on top of a 2D island of radius R satisfies the relation $\tau \ll \Delta t$. This relation also reflects on the island radius giving the relation $R \ll R_{cG}$ with R_{cG} given by

$$\frac{R_{cG}}{2a\nu'} = \frac{1}{F\pi R_{cG}^2} \mapsto R_{cG} = \sqrt[3]{\frac{2a\nu'}{F\pi}}. \quad (2)$$

Borrowing from metals [21] a value of ν' on the order of 10^6 Hz, from GaAs (001) [24] a value at 520°C for D of $2.24 \times 10^7 \text{ cm}^2 \text{ s}^{-1}$, and setting $F = 6 \times 10^{14} \text{ cm}^{-2} \text{ s}^{-1}$, $a = 3.25 \text{ \AA}$, we get values for R_{cD} and R_{cG} of $\sim 100 \text{ nm}$ and $\sim 45 \text{ nm}$,

respectively. Although these values are just indicative, because the used values of ν' and D are just educated guesses of what happens on AlGaAs(111)A surfaces, they anyway show a sort of internal consistency of our model. In fact, in addition to being both in a ‘‘reasonable’’ range for the phenomena we are considering, they are also of the same order of the average radius that can be inferred from the AFM measurements. The formation of a nucleus on the second layer requires, first, that (at least) two atoms are present on the island simultaneously, and, second, that the two meet before one of them escapes from the island.

Under the assumption $\tau_D \ll \tau \ll \Delta t$, the probability that an adatom, deposited at a time $t = 0$, is present on top of a 2D island, at a time t_1 later than the arrival time t_2 of a second atom, can be approximated as follows [21]:

$$\begin{aligned} P[t_1 > t_2] &= \frac{1}{\Delta t} \int_0^\infty P_{\text{res}}(t_1) dt_1 \int_0^{t_1} e^{-\frac{t_2}{\Delta t}} dt_2 \\ &\approx \frac{1}{\Delta t} \int_0^\infty t_1 P_{\text{res}}(t_1) dt_1 \approx \frac{\tau}{\Delta t}. \end{aligned} \quad (3)$$

In the case of strong step edge barriers the two atoms will almost certainly meet, because their residence time τ is much larger than the encounter time, which can be roughly identified with the diffusion time τ_D . The probability for a freshly deposited atom to form a nucleus is therefore equal to the probability that another atom is present on the island at its deposition. Multiplying this probability for the average arrival rate on the island top $\frac{1}{\Delta t}$, we get the rate

$$\omega = \frac{\tau}{\Delta t^2} = \frac{\pi^2 F^2 R^5}{2a\nu'} \quad (4)$$

that two adatoms are present at the same time on top of an island. The rate ω is intuitively proportional to the second-layer nucleation rate, except in the special case for which the critical nucleus $i^* = 1$ (two adatoms for nucleation). In this case in fact ω will be exactly equal to the second-layer nucleation rate and consequently Eq. (4) will return the value of the latter.

This rate changes very fast depending on island radius, passing for example (using the previously estimated values for ν' and D) from $\sim 10^{-3}$ Hz when $R = 1 \text{ nm}$, to a value of $\sim 10^2$ Hz at $R = 10 \text{ nm}$.

The dependence on growth parameters T and Φ in Eq. (4) is still hidden, and a few more steps are needed to make this dependence explicit. The dependence of the average radius R on the growth parameters can be given by the formula

$$R = R(F; \Phi; T; \Theta) = \sqrt[3]{\left(\frac{\mu V}{\rho}\right)} = \lambda \rho(F; \Phi; T; \Theta)^{-\frac{1}{3}}, \quad (5)$$

where λ is constant, V is the volume of group-III elements, the μ value depends on the island shape, ρ is the density of the islands, and Θ is the coverage. In order to evaluate the dependence of ρ on the growth parameter F , Φ , and T we extended Ref. [25] results, by including the effects of As flux via its influence on the Ga diffusion length. This has been done by adding a power dependence to the island density of the form Φ^q , with $q > 0$ as the effect of As flux is to reduce the Ga diffusion [24] and hence to increase the island density.

$$\rho(F; \Phi; T) \approx \xi(\Theta) F^p \Phi^q e^{\frac{E_n}{kT}}, \quad (6)$$

where $\xi(\Theta)$ is a function of the coverage Θ , $p < 1$ being Ga adatom kinetics in the complete condensation regime [25] and E_n is the nucleation energy. Our experiments were conducted at fixed coverage, so we can fix the $\Theta = \Theta_0$ and disregard the dependence on the coverage in the discussion. Using this expression in Eq. (5) the following relation for the average radius can be deduced:

$$R(F; \Phi; T) = \eta F^{-\frac{p}{3}} \Phi^{-\frac{q}{3}} e^{-\frac{E_n}{3kT}}, \quad (7)$$

where η is a constant. Inserting Eq. (7) in Eq. (4) and using the definition of ν' previously given, we can finally get

$$\omega(F, \Phi, T) \approx \alpha F^{2-\frac{5}{3}p} \Phi^{-\frac{5}{3}q} e^{\frac{3E_S-5E_n}{3kT}}, \quad (8)$$

where α is a constant. The island second-layer nucleation rate depends on two adatoms' coexistence at the island top; thus $\omega(F; \Phi; T)$ gives a direct access to the dependence of surface roughness on the growth parameters. It is worth noting that being $p < 1$ [25,26] we get that $\frac{5}{3}p < 2$, so that ω increases proportionally with the increasing of Ga flux F . The exponent q is always positive, being the effect of As flux to decrease group-III adatom diffusion [18,19].

B. Discussion of the results

A fundamental ingredient for the discussion is the knowledge of the parameters involved in the model, namely the two exponents p and q , the activation energy E_n , and the ES barrier energy E_S . The *a priori* knowledge of their values is precluded to us, being the growth dynamics too complex in the case of III-V compounds. However, by fitting the island density dependence on the growth conditions, we can obtain a direct measure of at least three of the four parameters involved, as ρ explicitly depends on T , F , and Φ [see Eq. (6)]. The obtained values are $E_n = 0.97 \pm 0.1$ eV, $p = 0.37 \pm 0.31$, and $p + q = 0.71 \pm 0.16$ from which we can infer that $q \approx 0.34$. It is worth noting that, despite the large error bar, the p value is in qualitative agreement with the expected exponent for the dependence on the Ga flux: $1 > p > 0.28$. Inserting the parameters in Eq. (8) it is possible to derive some general rules regarding the second-layer nucleation in different growth conditions. A little more algebra must be performed when looking for the dependence on the V/III ratio (Φ/F). In the case in which the ratio is varied at constant Φ we obtain $\omega \propto (\frac{\Phi}{F})^{\frac{5}{3}p-2}$ while in the opposite case (constant F) $\omega \propto (\frac{\Phi}{F})^{-\frac{5}{3}q}$.

(1) The second-layer nucleation increases with the increasing of Ga flux F , being the exponent $2 - \frac{5}{3}p$ always positive in the complete condensation regime, so that 3D growth is favored by higher F .

(2) The second-layer nucleation decreases with the increasing of As flux Φ , being q a positive quantity, so that 3D growth is hindered by higher Φ .

(3) The second-layer nucleation is a decreasing function of increasing V/III ratio, being the exponents $\frac{5}{3}p - 2$ and $-\frac{5}{3}q$ always negative, so that 3D growth is hindered by higher $\frac{\Phi}{F}$.

(4) The second-layer nucleation decreases with the increasing of temperature T , so that 3D growth is hindered by higher T , if $3E_S - 5E_n > 0$.

Following the considerations made at the end of the last subsection, we can interpret the morphological observations as a function of the growth parameters by means of Eq. (8). Concentrating our attention on the islands, we clearly see that our model well describes the experimental results, being the surface roughness an increasing function of F and a decreasing function of Φ and $\frac{\Phi}{F}$ (rules 1–3). In the temperature series (see Fig. 2) 3D growth is reduced for the islands by increasing the substrate temperature. This observation sets the ES energy value $E_S = E_D + \Delta E_S > 5/3E_n = 1.6$ eV (see rule 4). The value of E_D on GaAs(111)A is not available in the literature. We can have an estimate of it using theoretical calculations on GaAs(001) where $E_D \approx 1.5$ eV. The additional step edge barrier $\Delta E_S = E_S - E_D$ related to the ES edge effect is then expected to be larger than 100 meV.

However, when considering the actual overall surface roughness dependence on the growth conditions, we should pay attention to other factors that cannot be included in the ES model that has brought us to Eq. (8), such as extended defects and regime transitions.

A good starting point for such discussion is represented by the temperature series. Although the island population shows a reduction of the 3D growth with the increasing T , and consequently a lower rms at high temperatures, this is not what is observed on the surface overall. Hillock growth dynamics follows, in fact, a different behavior. The defect nature [18,19] of hillocks tends to promote second-layer nucleation and to increase their capture area proportionally to surface diffusion. This leads the morphological behavior of hillocks in the “opposite direction” with respect to what is expected for islands. However, this statement is not true for all the temperature range and adopting the strategy of decreasing the temperature in order to reduce the adatom diffusivity can be a bad choice. In fact, as previously reported, decreasing the temperature we may enter a growth regime (dendritic regime) where diffusivity is very low, the step edge reorganization processes are hindered, and the kinetic roughening dominates completely the final morphology.

This observation represents a crucial point. It demonstrates, in fact, that thinking on the transition from a 3D growth to a 2D-like only as a diffusion-limited process is too naive and in some ways also incorrect.

For what concerns the growth rate series, we can see again that, while islands follow the model prediction, which is an increase of the surface roughness with the increasing growth rate, the behavior of hillocks goes exactly in the opposite direction (see Figs. 5 and 6). The reason is the same discussed for the temperature series, that is, a change of the capture area of the hillocks with the growth conditions, although in this case the capture area of the hillocks is no longer determined by the adatom diffusion. In fact, increasing the growth rate we are also increasing the island density, due to the increased probability of the formation of islands above the critical nucleus size [25], thus reducing the inter-island distance well below the diffusion length. This increases the probability that an adatom is incorporated, during its diffusion, into a growing island, thus decreasing this way the adatom mean-free path. This effectively reduces the adatom island capture area to values that can be much lower than the one set by diffusivity only. As shown in Fig. 7, the effective mean-free path is set by

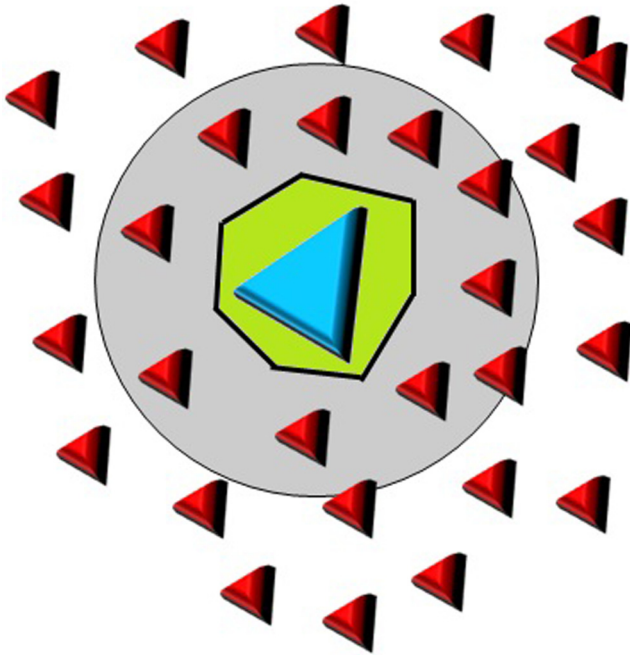


FIG. 7. Schematic picture of the reduction of the hillock's (large blue island at the center) capture area by adatom mean-free control via island (red triangles) density. The effective capture area of the hillock (the green Voronoi area around the hillock) can be strongly reduced, with respect to the one determined by the diffusivity (gray circle), by the presence of a high island density.

the average island-island distance, and this can be controlled by the island nucleation probability and thus, in turn, by the island density. This effect is clearly effecting strongly the hillock growth, as it is determined by the ability of the hillocks to accumulate material from the surroundings. The increase in group-III flux, while favoring the second-layer nucleation on the island's top, thus increasing island-related roughness, strongly limits the hillock's capture area, thus reducing hillock effects on the overall thickness.

As far as the V/III ratio series is concerned, it is worth noting that during the growth of this series the As flux was kept constant, while the group III was decreased in order to increase the V/III ratio. We observe that the density of islands decreases with rising V/III ratio but, contrary to what is seen in the the previous two series, the overall rms decreases too. Looking at Eq. (8) we can see that the island behavior follows what is stated by the model, that is, a decrease of second-layer nucleation with increasing (Φ/F) ratio. What is different from the previous series is that in this case also the hillock's height decreases with rising V/III ratio. The reason for this behavior can be ascribed to the fixed and high As flux. In fact, keeping the As flux constant at high values we are limiting the diffusivity of group-III adatom flux and thus, in turn, reducing the hillock's capture zone and hindering 3D growth on islands at the same time. Second-layer nucleation is, in fact, proportional to $\omega \propto (\frac{\Phi}{F})^{\frac{5}{3}p-2}$. The exponent $\frac{5}{3}p - 2$ is in fact always negative ($p < 1$).

It is therefore fundamental for the control of the GaAs (111)A surface roughness to find a balance between the

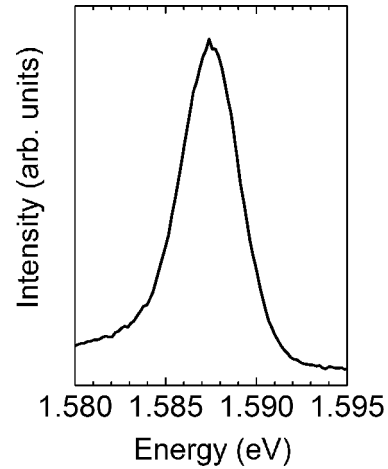


FIG. 8. Photoluminescence spectrum of the fabricated 5.5 nm GaAs/AlGaAs QW showing a full width at half maximum of 4.5 meV.

reduction of the effective mean-free path, obtained via both diffusion length reduction and increase of island density, and the increase of the second-layer nucleation, mostly controlled by group-III adatom flux.

C. Quantum well optical quality

The possibility to obtain extremely flat AlGaAs(111)A surfaces with rms below 0.2 nm opens up the fabrication of two-dimensional quantum nanostructures with extremely narrow emission. For this purpose we fabricated a 5.5 nm thick, strain-free GaAs/Al_{0.3}Ga_{0.7}As quantum well. We expect, in fact, the excitonic linewidth and the AlGaAs/GaAs/AlGaAs interface rms dL to be related by the equation [27]

$$dL \approx \frac{L dE_{ex}}{2(E_{ex} - E_g)}, \quad (9)$$

where L is the quantum well thickness, E_{ex} is the energy of the interband excitonic transition in the quantum well, E_g the energy gap of the quantum well material, and dE_{ex} the emission full width at half maximum. The emission spectrum of the fabricated quantum well is shown in Fig. 8. The well spectrum shows $E_{ex} = 1.587$ with $dE_{ex} = 4.5$ meV. Using the experimental values $L = 5.5$ nm, $E_{ex} = 1.587$ eV, and $E_g = 1.515$ eV in Eq. (9) we see that an emission broadening $dE_{ex} = 4.2$ meV corresponds to a well width fluctuation of $dL = 0.17$ nm, in perfect agreement with the roughness value < 0.2 nm measured by AFM.

This is a clear demonstration of how the high surface flatness control that can be reached by growth strategy and the procedures here presented strongly impacts the electronic properties of the quantum nanostructures realized on it. The quantum well in fact shows an extremely sharp emission of only 4.5 meV full width at half maximum [28].

V. CONCLUSIONS

We have presented a detailed study on how MBE growth parameters, namely temperature, growth rate, and V/III ratio, impact the growth dynamics of the Al_xGa_{1-x}As

($0 < x < 0.30$) (111)A surface. In particular we have identified and analyzed the factors that lead to huge overall roughness on this surface: (i) the presence of defect-induced hillocks; (ii) the island 3D growth. The latter has been often overlooked in previous studies, thus preventing the achievement of a truly atomically flat surface [18,19].

Our study has identified the Ehrlich-Schwöbel barrier as the leading factor on surface adatom dynamics. We then developed a theoretical model for the growth of III-V semiconductors in the presence of ES barriers. Within this framework we were able to interpret and control the island roughness. The hillocks' related roughness is controlled by shrinking their capture area through an efficient mechanism of reduction of adatom mean-free path via island density increase. This way we were able to drive the typical 3D growth of Ga(Al)As(111)A towards atomically flat surfaces

(<0.2 nm rms). Such low surface rms was obtained at a substrate temperature of 520°C , group-III flux of 0.5×10^{14} atoms $\text{s}^{-1} \text{cm}^{-2}$, and V/III ratio of 900. These growth conditions are quite far from those typical of (001) surfaces and are dictated by the necessity of suppressing hillocks' growth and promoting 2D growth of islands in the presence of a large Ehrlich-Schwöbel barrier. GaAs/Al_{0.30}Ga_{0.70}As quantum wells realized on such optimized surface show a record narrow emission linewidth of 4.5 meV.

The presented modeling of the growth dynamics on Ga(Al)As(111)A surfaces will permit us to obtain quantum nanostructures with extremely sharp interfaces, thus reducing excitonic emission broadening in QWs and carrier scattering at the interface in HMTs fabricated on (111)A substrates, thus opening to the possibility of fabricating high-efficiency HMTs and optoelectronic devices.

-
- [1] N. Miyata, H. Ishii, Y. Urabe, T. Itatani, T. Yasuda, H. Yamada, N. Fukuhara, M. Hata, M. Deura, M. Sugiyama, M. Takenaka, and S. Takagi, *Microelectron. Eng.* **88**, 3459 (2011).
- [2] M. Xu, Y. Q. Wu, O. Koybasi, T. Shen, and P. D. Ye, *Appl. Phys. Lett.* **94**, 212104 (2009).
- [3] M. K. Hudait, Y. Zhu, N. Jain, and J. L. Hunter, *J. Vac. Sci. Technol. B* **31**, 011206 (2013).
- [4] H. Li, T. Mei, G. Karunasiri, W. J. Fan, D. H. Zhang, S. F. Yoon, and K. H. Yuan, *J. Appl. Phys.* **98**, 054905 (2005).
- [5] D. Zhang, W. Lou, M. Miao, S.-c. Zhang, and K. Chang, *Phys. Rev. Lett.* **111**, 156402 (2013).
- [6] A. Hernandez-Minguez, K. Biermann, R. Hey, and P. V. Santos, *Phys. Rev. Lett.* **109**, 266602 (2012).
- [7] A. Balocchi, Q. H. Duong, P. Renucci, B. L. Liu, C. Fontaine, T. Amand, D. Lagarde, and X. Marie, *Phys. Rev. Lett.* **107**, 136604 (2011).
- [8] M. Q. Weng and M. W. Wu, *Phys. Rev. B* **88**, 195310 (2013).
- [9] H. Q. Ye, G. Wang, B. L. Liu, Z. W. Shi, W. X. Wang, C. Fontaine, A. Balocchi, T. Amand, D. Lagarde, P. Renucci, and X. Marie, *Appl. Phys. Lett.* **101**, 032104 (2012).
- [10] C. Zhao, J. Li, Y. Yu, H. Ni, Z. Niu, and X. Zhang, *Appl. Phys. Lett.* **104**, 052411 (2014).
- [11] T. Mano, M. Abbarchi, T. Kuroda, B. McSkimming, A. Ohtake, K. Mitsuishi, and K. Sakoda, *Appl. Phys. Express* **3**, 065203 (2010).
- [12] E. Stock, T. Warming, I. Ostapenko, S. Rodt, A. Schliwa, J. A. Toöfflinger, A. Lochmann, A. I. Toropov, S. A. Moshchenko, D. V. Dmitriev, V. A. Haisler, and D. Bimberg, *Appl. Phys. Lett.* **96**, 093112 (2010).
- [13] Y. H. Huo, A. Rastelli, and O. G. Schmidt, *Appl. Phys. Lett.* **102**, 152105 (2013).
- [14] K. F. Karlsson, M. A. Dupertuis, D. Y. Oberli, E. Pelucchi, A. Rudra, P. O. Holtz, and E. Kapon, *Phys. Rev. B* **81**, 161307 (2010).
- [15] M. A. Dupertuis, K. F. Karlsson, D. Y. Oberli, E. Pelucchi, A. Rudra, P. O. Holtz, and E. Kapon, *Phys. Rev. Lett.* **107**, 127403 (2011).
- [16] T. Kuroda, T. Mano, N. Ha, H. Nakajima, H. Kumano, B. Urbaszek, M. Jo, M. Abbarchi, Y. Sakuma, K. Sakoda, I. Suemune, X. Marie, and T. Amand, *Phys. Rev. B* **88**, 041306(R) (2013).
- [17] R. Singh and G. Bester, *J. Phys.: Conf. Ser.* **245**, 012008 (2010).
- [18] T. Uehara, T. Iwai, I. Yoshiba, and Y. Horikoshi, *Jpn. J. Appl. Phys.* **46**, 496 (2007).
- [19] Y. Horikoshi, T. Uehara, T. Iwai, and I. Yoshiba, *Phys. Status Solidi* **244**, 2697 (2007).
- [20] M. D. Johnson, C. Orme, A. W. Hunt, D. Graff, J. Sudijono, L. M. Sander, and B. G. Orr, *Phys. Rev. Lett.* **72**, 116 (1994).
- [21] T. Michely and J. Krug, *Islands, Mounds, and Atoms* (Springer Verlag, Berlin, 2004).
- [22] M. Einax, W. Dieterich, and P. Maass, *Rev. Mod. Phys.* **85**, 921 (2013).
- [23] G. Rosenfeld, B. Poelsema, and G. Comsa, *Chem. Phys. Solid Surf.* **8**, 66 (1997).
- [24] S. Bietti, C. Somaschini, L. Esposito, A. Fedorov, and S. Sanguinetti, *J. Appl. Phys.* **116**, 114311 (2014).
- [25] J. A. Venables, G. D. T. Spiller, and M. Hanbuechen, *Rep. Prog. Phys.* **47**, 399 (1984).
- [26] M. Sobanska, V. G. Dubrovskii, G. Tchutchulashvili, K. Klosek, and Z. R. Zytikiewicz, *Cryst. Growth Des.* **16**, 7205 (2016).
- [27] S. Sanguinetti, M. Guzzi, and M. Gurioli, in *Characterization of Semiconductor Heterostructures and Nanostructures*, edited by C. Lamberti (Elsevier, Amsterdam, 2008), pp. 175–208.
- [28] S. Cho, A. Sanz-Hervas, A. Majerfeld, and B. W. Kim, *Phys. Rev. B* **68**, 035308 (2003).